photonics

Communication

A Bound State in the Continuum Supported by a Trimeric Metallic Metasurface

Tao Fu, Ziyan Wang and Yonghe Chen *

Guangxi Key Laboratory of Precision Navigation Technology and Application, Guilin University of Electronic Technology, Guilin 541004, China
* Correspondence: yhchen@guet.edu.cn

Abstract: A bound state in the continuum (BIC) is a localized state in a continuous spectrum of radiating waves. In this study, the coupled-mode theory is introduced to more precisely interpret a symmetry-protected BIC and the quasi-BIC in a facile trimeric metasurface, compared with Fano formula, which is introduced to generate a high-quality factor resonance in a trimeric metallic slit metasurface. The multipole decomposition method and the near field distribution of the structure further illustrate that the underlying physics of the high-Q is mainly originated from the interference between the electric quadrupole mode and the magnetic toroidal mode. Physical mechanism shows that the resonance arises from the perturbation of symmetry-protected BICs. The result may play a role in the applications of lasers, optical sensors, and low-loss fibers.

Keywords: bound states in the continuum; metasurface; Fano's formula; coupled-mode theory; scattering power

check for updates

Citation: Fu, T.; Wang, Z.; Chen, Y. A Bound State in the Continuum Supported by a Trimeric Metallic Metasurface. *Photonics* **2023**, *10*, 40. https://doi.org/10.3390/photonics10010040

Received: 3 November 2022
Revised: 15 December 2022
Accepted: 29 December 2022
Published: 30 December 2022

Metasurfaces, composed of subwavelength structural units, can effectively manipulate the amplitude, phase, and polarization of the electromagnetic field within ultra-thin surfaces by designing the structure and material properties. In particular, metallic metasurfaces use the resonance of the localized surface plasmon to modulate the wavefront, which overcomes the shortcomings of traditional metamaterials such as large volume, high loss, and difficult processing, becoming a hot field in scientific research [1,2]. Recently, more and more attention has been paid to looking for the high-Q factor resonant structures of strong mode coupling [3–5]. In this regard, bound states in the continuum (BICs), combined with metasurfaces have arisen to bring forth a new idea that allows strong field confinement in a small mode volume [6]. Recent achievements have reported conspicuous applications such as lasers [7], slow-wave devices [8], and so on.

Bound states in the continuum (BICs) are wave solutions embedded in the radiative continuum, but are completely decoupled from it [9,10]. BICs were first proposed by von Neumann and Wigner in quantum mechanics, and have then been found in electromagnetic waves, acoustic waves in air, water waves, and elastic waves in solids [11]. The category of the BICs can be divided into Friedrich-Wintgen BICs, separated BICs, Fabry Perot BICs, and symmetry-protected BICs according to the realization principle of the bound states [12]. Most of the researches on metasurface BICs are based on the symmetry-protected BICs [13–16]. Symmetry-protected BICs can extract high-Q resonances by breaking the symmetry of the system and invoking a leakage channel in the form of Fano resonance [17–19].

Trimeric system metasurface supporting sharp Fano resonances was previously studied in various platforms, including all-dielectric and metallic structures [20]. Metal metasurfaces can enhance the near-field effect close the surface, trapping electromagnetic waves on the surface of the structure, thus boosting interactions between light and matter. However, the coupling method never further interprets the underlying physics of the high-Q quasi-BICs modes extracted from the symmetry-protected BICs by breaking the symmetry of the metasurface structure. In addition, the method of multipole decomposition and near field analysis clarifies the formation of the Fano resonance. The bandwidth and the resonant frequency of the transmission spectrum can be uniformly regulated with the change of asymmetric parameters. Symmetry-protected BICs in the metasurface possess promising applications in optics and photonics [21].

Figure 1a shows the trimeric slit geometry with a period of $p_x = p_y = p = 18.5$ mm. A gold metasurface was plated on a Poly tetra fluoroethylene (PTFE) substrate (thickness $t = 2.4$ mm, permittivity $\varepsilon = 2.55$ and loss tangent tan $\delta = 0.0002$). Each unit has three slits with different lengths but the same width $w = 2.2$ mm (shown in Figure 1b). The properties of the resonance were studied by using an asymmetry index $m = l/h$, where l and h are the length of the left slit and the others, respectively. The distance of the adjacent slits is $d = 3.7$ mm. The period of the unit cell should stay smaller than the resonance wavelength in the simulation process. The simulation was carried out by using the COMSOL Multiphysics® software under a plane wave with the electric field $\boldsymbol{E}_x$ propagate to -z direction (the background material is air $n = 1$). Perfectly matched layers boundary conditions are used to absorb the electromagnetic waves scattering to the free space. A typical Fano resonance curve appears in the transmission spectra when $m = 0.96$ in Figure 1c, the amplitude changed rapidly at the resonance peak and dip.

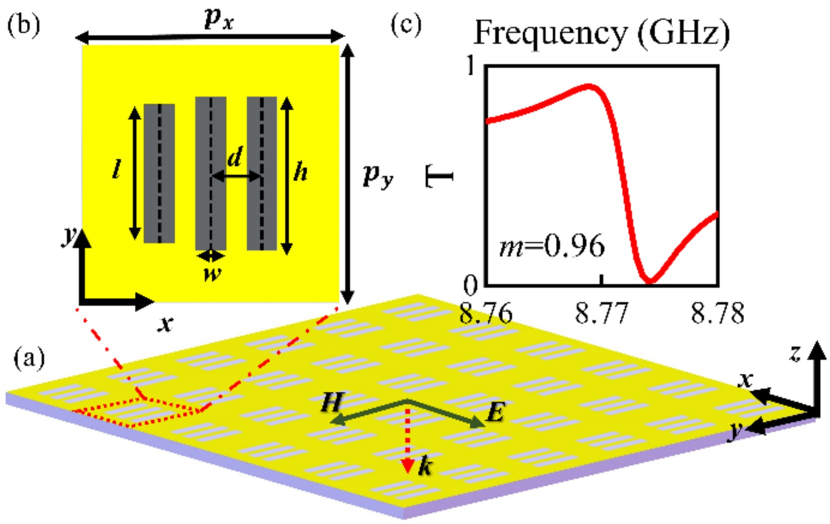

Figure 1. (**a**) Schematic of the trimeric metasurface and the electromagnetic field excitation, the red dashed box represents a unit of the metasurface shown in (**b**). (**c**) Normalized transmission spectra of the metasurface.

The resonant coupling can be transformed from BICs to quasi-BICs by breaking the symmetry of the metasurface and the quality factor can be extracted. Keeping the structure symmetry, the bound states will decouple from the radiation wave in free space due to the mismatch between the spatial symmetry of the localized mode and that of the external radiation wave, which is called the ideal BICs (the red dot circle indicated in Figure 2a). While breaking the symmetry of the structure, the bound state will separate from the continuous state, opening a leaky channel radiating energy into the free space. A sharp quasi-BICs as Fano resonance emerges from the transmission spectra and the bandwidth becomes wider as m deviates from 1. The Q-factor of the proposed system can reach up to 6×10^4 (in Figure 2b) and tends to infinity at the BIC point. The state of the BIC point is no longer leaky resonance; it becomes eigenmodes that do not decay.

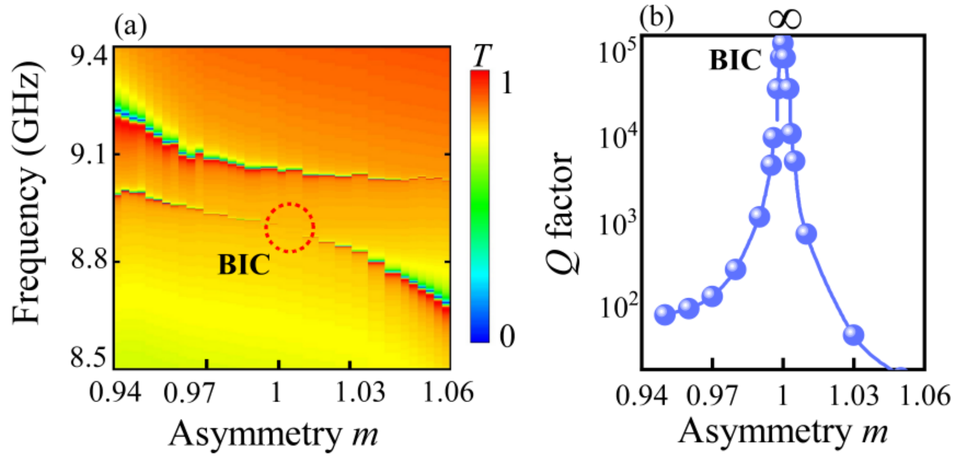

Figure 2. (**a**) The normalized transmission spectra with different asymmetry parameter m. The red dot circle represents the position of the BIC. (**b**) The quality factors as a function of asymmetry parameter m.

The multipole analysis and the near field distribution of the metasurface unit cell was used to reveal the intrinsic physical mechanism of the BIC mode. Figure 3a is the multipole decomposition of the transmission spectra, which clearly illustrate the contribution of each multipole moment to the total scattering power. The current distribution in the three slits structure shown as Equation (1) can be achieved [22],

$$\boldsymbol{J}(\boldsymbol{r}) = -i\omega\varepsilon_0(n^2-1)\boldsymbol{E}(\boldsymbol{r}) \tag{1}$$

where ***J(r)*** and ***E(r)*** represent the current density and electric field intensity in the Cartesian coordinate system at the internal point $\boldsymbol{r} = (x, y, z)$, ε_0 and n are the dielectric permittivity of the free-space and the complex refractive index from the material of the three stripes structure, respectively. The expressions of the moments and the scattered power corresponding to each multipole are shown in Table 1, where the δ and c denote the Dirac delta function and the speed of light, respectively. The subscripts α, β on behalf of the axis x, y, z in the Cartesian coordinates [23,24].

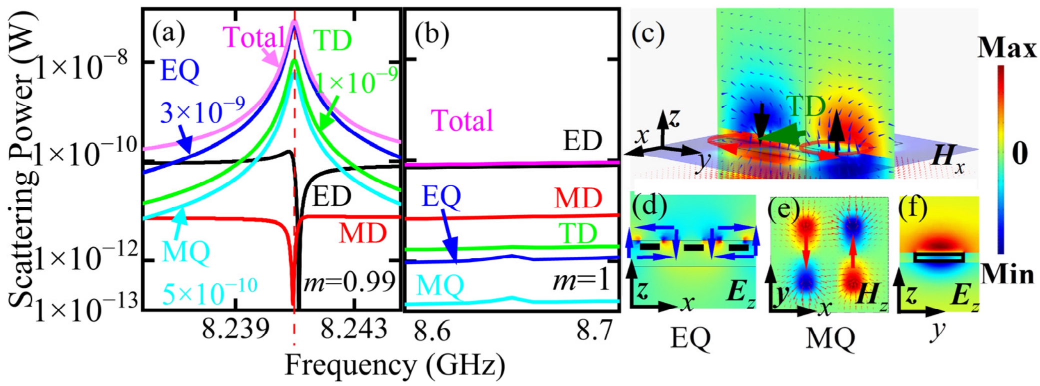

Figure 3. (**a**,**b**) Scattering power of logarithmic scale for multipoles moments with total scattering (pink line), ED (black line), MD (red line), TD (green line), EQ (deep blue line), and MQ (sky blue line) with m = 0.99 at around 8.24 GHz and m = 1, respectively. (**c**–**f**) are the nearfield profile of the metasurface, (**c**) the color maps of the $\boldsymbol{H_x}$, the black arrows and red arrows (include red circles) stand for the magnetic and electric field vectors, and the green arrow is the direction of the TD. (**d**) the deep blue arrows indicate the EQ, the three short black lines outline the three slits. (**e**) $\boldsymbol{H_z}$ in the x-y plane indicate the MQ, the arrows point in the direction of the magnetic field. (**f**) $\boldsymbol{E_z}$ in the y-z plane, the black box is the side view of the structure.

Table 1. Multipole's moments and corresponding far-field scattering power.

Multipole	Multipole Expression	Scattering Power
Electric dipole (ED)	$\boldsymbol{P} = \frac{1}{i\omega}\int \boldsymbol{J}(\boldsymbol{r})d^3r$	$I_P = \frac{2\omega^4}{3c^3}\lvert\boldsymbol{P}\rvert^2$
Magnetic dipole (MD)	$\boldsymbol{M} = \frac{1}{ic}\int (\boldsymbol{r} \times \boldsymbol{J}(\boldsymbol{r}))d^3r$	$I_M = \frac{2\omega^4}{3c^3}\lvert\boldsymbol{M}\rvert^2$
Toroidal dipole (TD)	$\boldsymbol{T} = \frac{1}{10c}\int \left[(\boldsymbol{r}\bullet\boldsymbol{J}(\boldsymbol{r}))\boldsymbol{r} - 2\boldsymbol{r}^2\boldsymbol{J}(\boldsymbol{r})\right]\boldsymbol{d}^3r$	$I_T = \frac{2\omega^6}{3c^5}\lvert\boldsymbol{T}\rvert^2$
Electric quadrupole (EQ)	$Q_{\alpha\beta} = \frac{1}{2i\omega}\int \left[\boldsymbol{r}_\alpha\boldsymbol{J}_\beta(\boldsymbol{r}) + \boldsymbol{r}_\beta\boldsymbol{J}_\alpha(\boldsymbol{r}) - \frac{2}{3}\delta_{\alpha,\beta}(\boldsymbol{r}\bullet\boldsymbol{J}(\boldsymbol{r}))\right]d^3r$	$I_{EQ} = \frac{\omega^6}{5c^5}\sum\left\lvert Q_{\alpha\beta}\right\rvert^2$
Magnetic quadrupole (MQ)	$M_{\alpha\beta} = \frac{1}{3c}\int \left[(\boldsymbol{r} \times \boldsymbol{J}(\boldsymbol{r}))_\alpha\boldsymbol{r}_\beta + (\boldsymbol{r} \times \boldsymbol{J}(\boldsymbol{r}))_\beta\boldsymbol{r}_\alpha\right]d^3r$	$I_{MQ} = \frac{\omega^6}{20c^6}\sum\left\lvert M_{\alpha\beta}\right\rvert^2$

The results of the multipolar decomposition depicted in Figure 3a show that the EQ, TD and MQ bound state modes are excited for m = 0.99. The scattering power of the EQ, TD and MQ contributes the first, second and third place to the resonance point around 8.24 GHz, respectively. Figure 3b shows they exist only when the structure is asymmetric, and interfere with the broader band ED mode that act as a continuum to form a narrow Fano resonance. In Figure 3c, a couple of MDs in the opposite directions form a TD (green arrow) pointed in the x-direction. The TD mode formed by the magnetic field was generated by the cyclic electric field. There are a pair of reverse EQs at the left and right slits, respectively, traced out by the deep blue arrows in Figure 3d. Figure 3e show the $\boldsymbol{H}_z$ in the x-y plane, indicating the MQ. The z component of the electric field $\boldsymbol{E}_z$ is shown in Figure 3f. Clearly the field becomes perfectly confined in the structure at the BICs point and does not couple to radiation. The coupling of the multipole modes caused by the asymmetric structure leads to spatial scattering and the observable quasi-BIC, while the strong locality of the electromagnetic field in the symmetric structure can realize strong energy confinement (the character of BIC).

Even though the multipoles analysis method qualitatively illustrated the BIC phenomenon, theories from Fano's formula [25] and coupled-mode theory [26,27] can thoroughly dig the physical mechanism of the resonance from the numerical results to be more reliable. Here, we show the comparison between the two methods. According to Fano's theory [28], the asymmetric curve of the transmission spectrum is from the interference between constructive and destructive of the narrow spectrum of discrete (localized) states, and the wide spectrum of continuous propagation modes. The transmission spectrum T can be modeled by the formula [29],

$$T = \frac{1}{1+q^2}\frac{(q+\Gamma)^2}{1+\Gamma^2} \tag{2}$$

where Γ defined by $2(E-E_0)/\gamma$ is the reduced energy, E_0 and γ are the energy and width of the resonance, respectively. $q = \cot\delta$ is the asymmetry parameter (δ represents the phase shift of modes), which is used to describe the degree of the asymmetry of the line shape. The curves of theoretical calculation from Fano's formula and simulation are shown as the red dotted lines and black lines in Figure 4a. The retrieved fitted parameters are depicted in Figure 4b. It can be seen that the γ is smaller as the structure has minor asymmetry, indicating that the resonance linewidth is narrow when the structure slightly deviates from symmetry. The fitting parameter q is of the order of unity; in this case both the continuous state and discrete state are of the same strength, causing the asymmetrical Fano line shapes. q has a minor change with varying m from 0.96 to 1.02 except 1, indicating that the Fano lines have the same "peak and dip" shape no matter what m parameters change. While the curves calculated by Fano's formula offset the simulation results (the green circles in Figure 4a) when m = 0.96 and m = 0.97, resulting in the fluctuations of the fitting parameters. Moreover, the fitting parameter curve can only reflect the changes of the degree of structural asymmetry, but the difference between structural symmetry and asymmetry is not obvious.

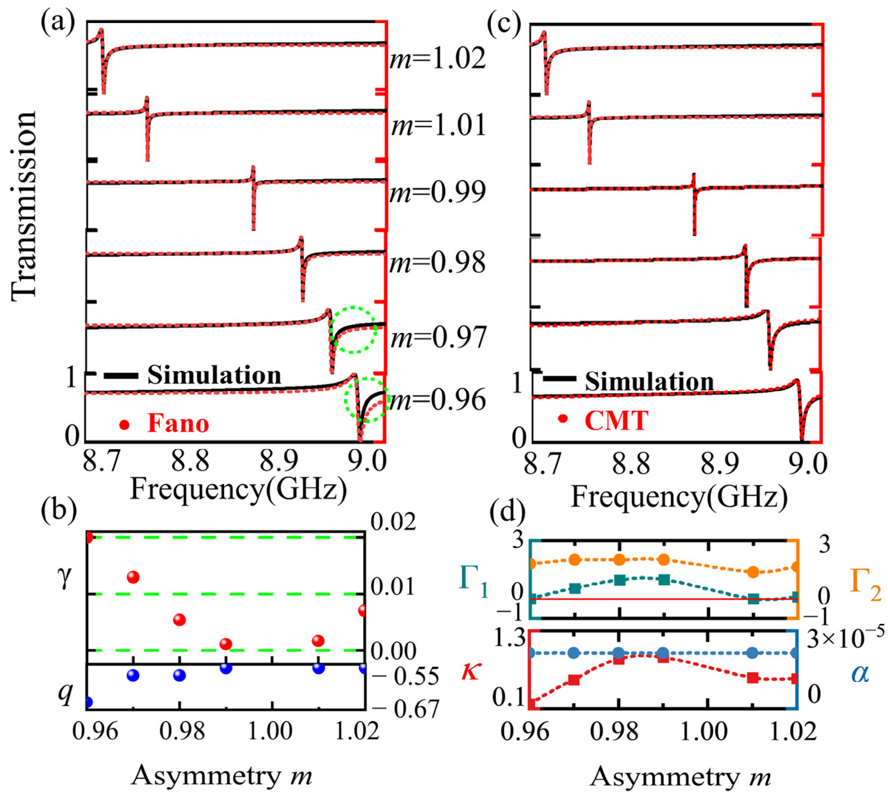

Figure 4. (**a**,**c**) the simulated (black dotted curves) and fitted (red dotted curves) transmission spectra with different m by Fano's formula and coupled-mode theory (CMT), respectively, the green circles show the deviation from the resonant points. (**b**,**d**) fitted parameters retrieved from Fano's formula and coupled-mode theory.

Based on this interpretation, the CMT was used to re-fit the simulated results (Figure 4c), which can express the general law of the coupling between multiple modes. Since the resonance is mainly formed by the electric quadrupole mode and toroidal mode, the two modes coupling system was used to fit our system, modeled by the formula [30]

$$t = \left| \frac{\Gamma_1}{\{-i[f - (f_0 + \kappa)]\Gamma_1 + \alpha\}} - \frac{\Gamma_2}{\{-i[f - (f_0 - \kappa)]\Gamma_2 + \alpha\}} \right| \tag{3}$$

where κ is the near-field coupling coefficient, which describes the coupling intensity of the two modes and depends on the degree of the symmetry sensitively. Γ_1 and Γ_2 are the radiation decay rate of eigen-frequencies of the two collective modes as mentioned above, and their magnitude affects the resonance bandwidth of the transmission spectrum. α and f_0 are the absorptive decay rate and the resonance frequency point, respectively. The radiation decay rate of the two modes decreases and the resonance bandwidth narrows when the structure turns to symmetry, shown in Figure 4d. Γ_1 approaches to 0 with the maximum value κ at m approaches to 1 (the red line shows the 0-label line), indicating that there is intensive coupling while no energy is radiating into free space. The symmetric structure results in the disappearance of the resonance bandwidth and the formation of an infinite Q-factor. Combined with the disappeared resonance bandwidth, the reason for the formation of BIC is illustrated. α keeps small throughout the fitting process. Clearly, the results calculated by the coupled-mode theory can not only be highly consistent with the simulation results at the resonant peaks and dips of all parameters, but also highlights the obvious transition between BIC and quasi-BIC.

In conclusion, we employed a metasurface to achieve high-Q quasi-BICs modes from the symmetry-protected BICs. The metasurface unit cell is composed of trimeric metallic slits that support Fano resonances produced by the coupling of the electric quadrupole and magnetic toroidal dipole. The bound states decoupled from the radiation wave in the symmetric structure and form a strong locality of electromagnetic field, which can realize strong energy confinement. A leaky channel radiating energy opened into the free space in the asymmetric structure, realizing the transformation of BICs and quasi-BICs. Fano's formula elaborates the changes in the degree of structural asymmetry well, but fails to show the difference between structural symmetry and asymmetry. This prompted us to revisit the same problem using the coupled-mode theory. By introducing the two-mode CMT, the physical mechanism of the transition between BIC and quasi-BIC can be highlighted. The high-Q quasi-BIC obtained by our system can be used for many applications, such as ultrasensitive sensors, nonlinear metasurface and compact lasing devices [31–33].

Author Contributions: Conceptualization, T.F.; writing—original draft preparation, Z.W.; supervision, Y.C. All authors have read and agreed to the published version of the manuscript.

Funding: This research was funded by the National Natural Science Foundation of China (11965009), Natural Science Foundation of Guangxi (2018GXNSFBA050052, 2018AD19057), Innovation Project of Guangxi Graduate Education (YCSW2021183).

Informed Consent Statement: Informed consent was obtained from all subjects involved in the study.

Data Availability Statement: The data presented in this study are available on request from the author.

Conflicts of Interest: The authors declare no conflict of interest.

References

1. He, J.; Zhang, Y. Metasurfaces in terahertz waveband. *J. Phys. D Appl. Phys.* **2017**, *50*, 464004. [CrossRef]
2. Deng, Z.-L.; Shi, T.; Krasnok, A.; Li, X.; Alù, A. Observation of localized magnetic plasmon skyrmions. *Nat. Commun.* **2022**, *13*, 8. [CrossRef] [PubMed]
3. An, Y.; Fu, T.; Liu, Q.; Ouyang, Z. High-Q Fano resonance based on degenerate modes in a single dielectric point-defect photonic crystal cavity with x–y asymmetry. *Appl. Phys. Express* **2020**, *13*, 032006. [CrossRef]
4. Amin, M.; Ramzan, R.; Siddiqui, O. Fano resonance based ultra high-contrast electromagnetic switch. *Appl. Phys. Lett.* **2017**, *110*, 181904. [CrossRef]
5. Pu, M.; Hu, C.; Huang, C.; Wang, C.; Zhao, Z.; Wang, Y.; Luo, X. Investigation of Fano resonance in planar metamaterial with perturbed periodicity. *Opt. Express* **2013**, *21*, 992–1001. [CrossRef]
6. Liu, Z.; Xu, Y.; Lin, Y.; Xiang, J.; Feng, T.; Cao, Q.; Li, J.; Lan, S.; Liu, J. High-Q Quasibound States in the Continuum for Nonlinear Metasurfaces. *Phys. Rev. Lett.* **2019**, *123*, 253901. [CrossRef]
7. Wang, X.; Duan, J.; Chen, W.; Zhou, C.; Liu, T.; Xiao, S. Controlling light absorption of graphene at critical coupling through magnetic dipole quasi-bound states in the continuum resonance. *Phys. Rev. B* **2020**, *102*, 155432. [CrossRef]
8. Doeleman, H.M.; Monticone, F.; den Hollander, W.; Alù, A.; Koenderink, A.F. Experimental observation of a polarization vortex at an optical bound state in the continuum. *Nat. Photonics* **2018**, *12*, 397–401. [CrossRef]
9. Hsu, C.W.; Zhen, B.; Stone, A.D.; Joannopoulos, J.D.; Soljačić, M. Bound states in the continuum. *Nat. Rev. Mater.* **2016**, *1*, 16048. [CrossRef]
10. Yesilkoy, F.; Arvelo, E.R.; Jahani, Y.; Liu, M.; Tittl, A.; Cevher, V.; Kivshar, Y.; Altug, H. Ultrasensitive hyperspectral imaging and biodetection enabled by dielectric metasurfaces. *Nat. Photonic* **2019**, *13*, 390–396. [CrossRef]
11. Han, S.; Cong, L.; Srivastava, Y.K.; Qiang, B.; Rybin, M.V.; Kumar, A.; Jain, R.; Lim, W.X.; Achanta, V.G.; Prabhu, S.S.; et al. All-Dielectric Active Terahertz Photonics Driven by Bound States in the Continuum. *Adv. Mater.* **2019**, *31*, e1901921. [CrossRef]
12. Bogdanov, A.A.; Koshelev, K.L.; Kapitanova, P.V.; Rybin, M.V.; Gladyshev, S.A.; Sadrieva, Z.F.; Samusev, K.B.; Kivshar, Y.S.; Limonov, M.F. Bound states in the continuum and Fano resonances in the strong mode coupling regime. *Adv. Photonics* **2019**, *1*, 016001. [CrossRef]
13. Koshelev, K.; Lepeshov, S.; Liu, M.; Bogdanov, A.; Kivshar, Y. Asymmetric Metasurfaces with High-Q Resonances Governed by Bound States in the Continuum. *Phys. Rev. Lett.* **2018**, *121*, 193903. [CrossRef]
14. Tittl, A.; Leitis, A.; Liu, M.; Yesilkoy, F.; Choi, D.Y.; Neshev, D.N.; Kivshar, Y.S.; Altug, H. Imaging based molecular barcoding with pixelated dielectric metasurfaces. *Science* **2018**, *360*, 1105–1109. [CrossRef]
15. Koshelev, K.; Kruk, S.; Melik-Gaykazyan, E.; Choi, J.H.; Bogdanov, A.; Park, H.G.; Kivshar, Y. Subwavelength dielectric resonators for nonlinear nanophotonics. *Science* **2020**, *367*, 288–292. [CrossRef]
16. Cong, L.; Singh, R. Symmetry-Protected Dual Bound States in the Continuum in Metamaterials. *Adv. Opt. Mater.* **2019**, *7*, 1900383. [CrossRef]
17. Deng, Z.-L.; Li, X.; Fu, T.; Wang, G.P. Fano Resonance in a Metasurface Composed of Graphene Ribbon Superlattice. *IEEE Photonics J.* **2017**, *9*, 4801107. [CrossRef]

18. Limonov, M.F.; Rybin, M.V.; Poddubny, A.N.; Kivshar, Y.S. Fano resonances in photonics. *Nat. Photonics* **2017**, *11*, 543–554. [CrossRef]
19. Fang, C.; Yang, Q.; Yuan, Q.; Gan, X.; Zhao, J.; Shao, Y.; Liu, Y.; Han, G.; Hao, Y. High Q resonances governed by the quasi-bound states in the continuum in all-dielectric metasurfaces. *Opto-Electron. Adv.* **2021**, *4*, 200030. [CrossRef]
20. Fu, T.; Liu, F.; An, Y.; Li, Q.; Li, H.; Sun, T.; Xiao, G.; Muhammad, N. Separately tuning of double Fano resonances in facile asymmetric slit metasurface. *Appl. Phys. Express* **2020**, *13*, 052009. [CrossRef]
21. Kim, S.; Kim, K.H.; Cahoon, J.F. Optical Bound States in the Continuum with Nanowire Geometric Superlattices. *Phys. Rev. Lett.* **2019**, *122*, 187402. [CrossRef] [PubMed]
22. Yang, Z.J.; Zhao, Q.; He, J. Fano interferences of electromagnetic modes in dielectric nanoblock dimers. *J. Appl. Phys.* **2019**, *125*, 063103. [CrossRef]
23. Manna, U.; Sugimoto, H.; Eggena, D.; Coe, B.; Wang, R.; Biswas, M.; Fujii, M. Selective excitation and enhancement of multipolar resonances in dielectric nanospheres using cylindrical vector beams. *J. Appl. Phys.* **2020**, *127*, 033101.
24. Luk'Yanchuk, B.; Zheludev, N.I.; Maier, S.A.; Halas, N.J.; Nordlander, P.; Giessen, H.; Chong, C.T. The Fano resonance in plasmonic nanostructures and metamaterials. *Nat. Mater.* **2010**, *9*, 707–715. [CrossRef] [PubMed]
25. Rybin, M.V.; Khanikaev, A.B.; Inoue, M.; Samusev, K.B.; Steel, M.J.; Yushin, G.; Limonov, M.F. Fano resonance between Mie and Bragg scattering in photonic crystals. *Phys. Rev. Lett.* **2009**, *103*, 023901. [CrossRef]
26. Guo, H.; Lin, J.; Qiu, M.; Tian, J.; Wang, Q.; Li, Y.; Sun, S.; He, Q.; Xiao, S.; Zhou, L. Flat optical transparent window: Mechanism and realization based on metasurfaces. *J. Phys. D Appl. Phys.* **2018**, *51*, 074001. [CrossRef]
27. Hsu, C.W.; DeLacy, B.G.; Johnson, S.G.; Joannopoulos, J.D.; Soljacic, M. Theoretical criteria for scattering dark states in nanostructured particles. *Nano Lett.* **2014**, *14*, 2783–2788. [CrossRef]
28. Miroshnichenko, A.E.; Flach, S.; Kivshar, Y.S. resonances in nanoscale structures. *Rev. Mod. Phys.* **2010**, *82*, 2257–2298. [CrossRef]
29. Huang, W.; Lin, J.; Qiu, M.; Liu, T.; He, Q.; Xiao, S.; Zhou, L. A complete phase diagram for dark-bright coupled plasmonic systems: Applicability of Fano's formula. *Nanophotonics* **2020**, *9*, 3251–3262. [CrossRef]
30. Yang, B.; Liu, T.; Guo, H.; Xiao, S.; Zhou, L. High-performance meta-devices based on multilayer meta-atoms: Interplay between the number of layers and phase coverage. *Sci. Bull.* **2019**, *64*, 823–835. [CrossRef]
31. Koshelev, K.; Tang, Y.; Li, K.; Choi, D.-Y.; Li, G.; Kivshar, Y. Nonlinear Metasurfaces Governed by Bound States in the Continuum. *ACS Photonics* **2019**, *6*, 1639–1644. [CrossRef]
32. Shi, T.; Deng, Z.-L.; Tu, Q.-A.; Cao, Y.; Li, X. Displacement-mediated bound states in the continuum in all-dielectric superlattice metasurfaces. *PhotoniX* **2021**, *2*, 7. [CrossRef]
33. Wang, W.; Yan, H.; Xiong, L.; Zheng, L. Symmetry-protected bound state in the continuum in the metasurface of dielectric nanodisk with the inclined surface. *J. Mod. Opt.* **2021**, *68*, 699–706. [CrossRef]